Noname manuscript No.
(will be inserted by the editor)

Effect of size distribution on mixing of a polydisperse wet granular material in a belt-driven enclosure

Pallab Sinha Mahapatra · Sam Mathew · Mahesh V. Panchagnula · Srikanth Vedantam

the date of receipt and acceptance should be inserted later

Abstract We use a recently developed coupled fluid-particle discrete element model to study mixing of a wet granular material in a two dimensional setting. The particles are modeled as linearly elastic disks and are considered to be immersed

Pallab Sinha Mahapatra

Department of Applied Mechanics, Indian Institute of Technology Madras, Chennai 600 036 India.

Present address: Department of Mechanical and Industrial Engineering, University of Illinois at Chicago, Chicago 60607 USA

E-mail: pallabju@gmail.com

Sam Mathew · Mahesh V. Panchagnula

Department of Applied Mechanics, Indian Institute of Technology Madras, Chennai 600 036 India

E-mail: sam.cfd.iitm@gmail.com; mvp@iitm.ac.in

Srikanth Vedantam

Department of Engineering Design, Indian Institute of Technology Madras, Chennai 600 036 India

E-mail: srikanth@iitm.ac.in

in a Newtonian fluid. The fluid-particle interaction is modeled using a linear drag model under the assumption that the fluid inertia is small compared to particle inertia. The granular slurry is driven by a belt moving at constant velocity in a square cavity. In the simulations, we consider three types of size distributions: monodisperse, bidisperse with several particle size ratios, and polydisperse Gaussian distributions with several different standard deviations. Mixing is characterized using both strong and weak measures. Size segregation is observed only in the bidisperse simulations. The energy required for mixing polydisperse slurries decreases with increasing standard deviation of the particle sizes. Finally, we show the benefits of engineering certain polydisperse particle size distributions towards minimizing energy consumption.

1 Introduction

The flow of granular materials has been widely studied for several decades due to their scientific and technological importance. Mixing and segregation in granular flows is particularly important in many industrial applications. The role of size polydispersity on mixing and segregation has been studied through experiments [1] and by modeling [2]. An interstitial fluid such as air plays a minor role in the mechanics of the dry granular flows [3–8]. On the other hand, an interstitial fluid such as water or oil plays a significant role in the mechanics of *wet* granular flows. While wet granular flows have been just as important from the industrial viewpoint, there have been far fewer studies on the mixing of such materials. The main reason for the paucity of such studies is the difficulty in coupling the fluid and particle interactions in a tractable manner.

The presence of a small amount of liquid within the granular material only increases the cohesive forces in the granular system [9]. On the other hand, if the grains are fully immersed due to a larger amount of the liquid, the wet granular material is called a slurry [10]. Fully immersed wet granular slurry flows occur in the food industry, geological flows and in construction. In some industrial sectors like chocolate and pharmaceuticals manufacturing, the flows may be in the presence of a highly viscous interstitial fluid.

Several experimental studies have investigated the dynamics of wet granular materials. Granular slurries have been studied in a 2D vibrated bed [9, 11], as flows down inclines [12] and in circular rotating drums [13, 14]. With the decrease of the volume of interstitial liquid, the role of liquid viscosity is greatly altered. There have been fewer studies of the mechanics of such dense wet granular flows. Models of granular slurries have been proposed by considering one-way coupling [15, 16] and two-way coupling between the interstitial fluid and the particles [13]. The flow of granular particles in a lid driven cavity has also been studied in [17, 18]. Numerical studies of slurry flows have been generally few in number due to the complexity in modelling coupled fluid-particle behavior. Recently, Bonkinpillewar et al. [19] have developed a simple and computationally tractable model of wet granular systems. The validity of the model is restricted to regimes where the fluid inertia is small compared to the particle inertia in any representative volume element. This assumption is satisfied in dense granular slurries in which the particle density is large compared to the fluid density and thus encompasses many flows of practical interest.

In this work we have considered a 2D system with an expectation that the basic behavior will not change for 3D systems with unidirectional belt

motion. During simulations or processing images of experiments, most researchers assume mixing to be a 2D phenomenon. When the third dimension is small (of the order of the particle diameter) and the driving conditions are such that secondary flows are not induced, we consider the 2D setting to be realistic. The dynamics of mixing and segregation of a binary mixture of glass beads and coriander seeds were studied by Rodriguez et al. [20] in a quasi 2D pile. They have assumed that the grains were layered uniformly in all radial direction of the 3D pile. Misra and Poorsolhjouy [21] studied the instability and stress-strain behavior of cylindrical particles in 2D regular assemblies. The width of the plate was taken small during the experiment and hence they have assumed a 2D framework for their modeling. Hsiau et al. [11] experimentally investigated the effects of the addition of liquid content, viscosity, and surface tension on dynamic properties of wet particulates in a 2D wet vibrated granular bed. On the other hand, when there exists an open surface and the flow front changes its direction spontaneously researchers have considered 3D system, for example, particle fluid motion in a rotating drum [22–24].

In industrial applications, granular materials are usually polydisperse. In addition, segregation of particles in polydisperse mixtures often occurs during handling or transportation and can lead to undesired product quality. Segregation of particles can happen due to differences in particle sizes and other physical properties which may affect the behavior of the granular flows. There is great interest in analyzing the segregation processes in different geometries [4]. The effect of size distribution of polydisperse granular flows has been found to be very important in dry granular flows. Experiments by Jain et al. [25] indicate that enhanced mixing

and reduced segregation occur in binary and ternary mixtures with a size distribution of the particles. The amount of segregation has also been observed to reduce with an increase of mass fraction of intermediate species present in the system. Pereira and Cleary [14] studied the segregation of mixtures composed of dry particles having either different sizes or density in rotating tumblers. Mixing and segregation of multi component dry mixtures has also been reported by references [6, 8]. DEM models have been used to simulate the mixing of bidisperse dry granular particles as well as polydisperse dry granular flows [26, 27]. As mentioned earlier, such extensive studies have not been performed in slurry flows.

In the present work we employ a DEM proposed by Bonkinpillewar et al. [19] to study mixing of mono- and poly-disperse wet granular materials in a square cavity. The grains are modeled as soft disks and the elastic collision between the grains are assumed to follow the Hertz model. The fluid medium exerts a linear drag on the particles which is taken to be proportional to the relative velocity of the particle and the fluid medium at the particle location. Due to the assumption that the fluid inertia is small compared to the particle inertia in any representative area element, the velocity of the fluid is calculated as a weighted average of the particle velocities in a neighborhood. A detailed description of the method can be found in [19]. **The present work deals with modeling the dynamics of dense granular slurries (near the random packing limit). The inter particle collision time interval in such a system is small and solving the hydrodynamics while accounting for the collisions is still computationally prohibitive. Our modeling approach is intended to fill this gap and allows the user to perform device-scale simulations. For large scale parametric studies, we hope that this model will prove useful to designers with the exception of low volume**

concentrations. In this work we have focused on understanding the mixing of mono-disperse, bidisperse and polydisperse wet granular particles in a lid driven enclosure. The polydisperse system is taken to contain uniform size distribution and Gaussian distributions. To the best of author's knowledge the effect of polydispersity on wet granular mixing inside a belt driven enclosure has not been studied before. In the following section, the equations governing the model are briefly described following [19] and the numerical solution procedure is described in detail. Two measures of mixing are considered and described in Sec. 2. The results of the simulations are presented in Sec. 3. The monodisperse, bidisperse and polydisperse results are presented in juxtaposition for comparison.

2 Numerical approach details

2.1 Model description

In this section, we briefly summarize the model presented in Bonkinpillewar et al. [19]. The model is applicable to fully immersed wet granular slurries. The fluid medium is considered to be viscous and the fluid inertia is assumed to be small in comparison to the particle inertia. The model incorporates the interaction of particles with each other and with the walls through Hertzian contact forces [28] which, in a two dimensional setting, is a linear soft sphere model. The particles experience a drag due to the fluid medium which is modeled by Stokes' drag and is taken to be linearly proportional to velocity of the particle relative to the velocity of the fluid medium at that point. The velocity of the fluid is not explicitly calculated, but is taken to be a weighted average of the surrounding particle velocities [29]. In

addition, a uniform gravity field is simulated by a constant force applied to each particle, directed vertically downwards.

The total force on a particle is given by

$$\mathbf{F} = \mathbf{F}_{pp} + \mathbf{F}_d + m\mathbf{g} \tag{1}$$

The interparticle interaction force ($\mathbf{F}_{pp}$) is taken to be of a linear soft-sphere form

$$\mathbf{F}_{pp} = \begin{cases} -k_n \boldsymbol{\delta} & |\boldsymbol{\delta}| > 0 \\ \mathbf{0} & otherwise \end{cases} \tag{2}$$

where $\boldsymbol{\delta} = \left(\left|\mathbf{r}_i - \mathbf{r}_j\right| - ((d_i + d_j)/2)\right) \frac{\mathbf{r}_i - \mathbf{r}_j}{|\mathbf{r}_i - \mathbf{r}_j|}$, is the separation of two particles i and j in terms position vectors $\mathbf{r}_i$ and $\mathbf{r}_j$ and diameters d_i and d_j). The direction of the force on a given particle is along the line joining the particle centers. The coefficient k_n is related to the elastic modulus of the particle material using Hertz theory.

The equation for drag on a particle (i) is motivated by Stokes' drag and taken to be proportional to relative velocity between a particle and the fluid at the same location [30].

$$\mathbf{F}_{d,i} = C_v d_i \left(\mathbf{v}_{p,i} - \mathbf{v}_i\right) \tag{3}$$

where, C_v is a hydrodynamic drag coefficient **similar to the drag coefficient** $3\pi\mu$ **of the Stokes' law (**μ **is the fluid viscosity)**, $\mathbf{v}_i$ is the velocity of particle i and $\mathbf{v}_{p,i}$ is the velocity of the surrounding fluid determined from a weighted mean of surrounding particles. The relative velocity is determined using a newly proposed weighted function based on n neighboring particles surrounding the i^{th} particle:

$$\mathbf{v}_{p,i} = \frac{\sum_{j=1}^{n} m_j W_{ij} \left(\left\|\mathbf{r}_i - \mathbf{r}_j\right\|, h_i\right) \mathbf{v}_j}{\sum_{j=1}^{n} m_j W_{ij} \left(\left\|\mathbf{r}_i - \mathbf{r}_j\right\|, h_i\right)} \tag{4}$$

where the weighing function W_{ij} is a Gaussian given by

$$W_{ij} = \begin{cases} exp\left(-\eta \frac{\|\mathbf{r}_i - \mathbf{r}_j\|^2}{{h_i}^2}\right) & \frac{\|\mathbf{r}_i - \mathbf{r}_j\|}{h_i} \leq 1 \\ 0 & otherwise \end{cases} \tag{5}$$

and h_i is a radius of influence for particle i which corresponds to the extent to which the particle's neighborhood influences its surrounding fluid velocity. Finally, m_i is the mass of the i^{th} particle. In this study, we set $h = 5d$. A constant η defines the standard deviation of the Gaussian distribution and is taken as 2 in our simulations as suggested by Drumm et al. [29]. The calculated fluid velocity, $\mathbf{v}_{p,i}$ is taken to be zero if there are no surrounding particles in the neighborhood. This is consistent with the assumption that fluid inertia is small in comparison to particle inertia.

2.2 Simulation details

The simulations in this work are in a two dimensional square domain of side 40 cm. Disks of diameter 5 mm are initially packed at 74% area fraction in a square lattice. The walls of the domain are modeled by fixed disks of the same size as the particles. In the monodisperse case, the domain is filled with 6084 particles. Three cases are considered for the bidisperse simulations by introducing a second set of particles of diameter 2.5 mm at different number concentrations (5%, 25% and 50%). In the polydisperse case, particles with uniform size distribution and Gaussian size distributions are considered with a mean diameter $d_m = 5$ mm. Different cases with standard deviations σ were considered, with σ/d_m values ranging from 1% to 10%. In all the simulations the same packing fraction was maintained. The belt driving the flow is placed at the bottom of the cavity and is composed of particles

of the same size as the granular particles. These belt particles are collectively moved at a constant speed.

The equations of motion based on the algebraic sum of the forces on each particle are solved numerically for the position and velocity as a function of time using the Velocity-Verlet algorithm [31]. The three steps in the Velocity-Verlet algorithm are

1. Position update: $\mathbf{x}(t+\Delta t) = \mathbf{x}(t) + \mathbf{v}(t)\Delta t + \frac{1}{2}\mathbf{a}(t)\Delta t^2$
2. New acceleration: $\mathbf{a}(t+\Delta t) = \frac{\mathbf{F}_{net}(t+\Delta t)}{m}$, using the new position, $x(t+\Delta t)$, from step 1
3. Velocity update: $\mathbf{v}(t+\Delta t) = \mathbf{v}(t) + \frac{1}{2}\left[\mathbf{a}(t) + \mathbf{a}(t+\Delta t)\right]\Delta t$

In the above algorithm, determining the forces on the particles at each time step is the most computationally intensive part. According to the Velocity-Verlet algorithm, the force on each particle needs to be calculated twice at each time step. A linked list algorithm is employed to reduce the computational effort [32] and to obtain accurate solutions.

2.3 Mixing and order quantification

Doucet et al. [33] have proposed weak and strong sense mixing parameters (β_{ws} and β_{ss}, respectively) based on the degree of correlation of current particle positions with respect to each of their initial coordinates (spatial and/or size dimensions). The weak sense mixing parameter (β_{ws}) only depends on the particle position relative to its initial location. For weak sense mixing, the distribution of particles at time t is independent of the initial distribution. As such, the two distributions are not correlated. On the other hand, the parameter quantifying mixing in the

strong sense β_{ss} includes the effect of particle sizes. In other words, it means that the distribution of particles at time t is independent of the initial distribution with respect to both space and properties. These parameters are determined based on a Principal Component Analysis (PCA) of the particle positions and size data.

The detailed procedure for these mixing indices has been explained by Doucet et al. [33]. The particles in the current problem are described by two spatial coordinates and one size coordinate. Following Doucet et al. [33], we describe the determination of the mixing indices

1. The particles positions and diameter coordinates at initial instant, $t = 0$ are scaled based on the variance and mean.
2. The particles positions and diameter coordinates at future instants of time, t are scaled based on the instantaneous variance and mean.
3. Computing the correlation matrix $\rho({X_i}^t, {X_j}^0)$, where $i = 1, 2$, and $j = 1, 2, 3$. X_1 and X_2 is the list of x and y coordinates of the particles and is a N-row matrix (N being the number of particles), X_3 corresponds to the size dimension. By definition, the correlation matrix involves the product of the transpose of $({X_i}^t)$ and $({X_j}^0)$, t and 0 denoting time instants.
4. Creating the correlation matrix C, by assigning $C_{ij} = \rho({X_i}^t, {X_j}^0)$.
5. Computing matrix M, such that, $M = CC^T$. M is now a symmetric matrix
6. Determining for M, the maximum eigenvalue λ and the corresponding eigenvector α. The solution of the eigenvalue problem $\alpha M = \lambda\alpha$ allows the construction of eigenvectors.
7. The weak sense mixing parameter for two-dimensional space is defined as,

$$\beta_{ws} = \sqrt{\lambda_{ws}/2} \tag{6}$$

where λ_{ws} corresponds to the eigenvalue of the matrix M, which is constructed from the correlation matrix C, such that, $C_{ij} = \rho({X_i}^t, {X_j}^0)$, and $i, j = 1, 2$, i.e., only spatial correlation is considered. The weak sense mixing parameter therefore, misses the size segregation effects.

8. The strong sense mixing parameter for two-dimensional space and additional size coordinate is defined as,

$$\beta_{ss} = \sqrt{\lambda_{ss}/3} \tag{7}$$

λ_{ss} corresponds to the eigenvalue of the matrix M, which is constructed from the correlation matrix C, such that, $C_{ij} = \rho({X_i}^t, {X_j}^0)$, and $i = 1, 2$, while $j = 1, 2, 3$, as described above.

The fluidity of the granular material has been quantified based on so-called local and global order parameters proposed by Mermin [34]. The local order parameter is based on the polar orientation of the neighboring particles surrounding a given particle. The local order parameter ψ_i for a particle i is given by

$$\psi_i = \frac{\sum_{k=1}^{n_{nb}} e^{j6\alpha}}{n_{nb}} = \frac{1}{n_{nb}} \sum_{k=1}^{n_{nb}} [cos(6\alpha) + j\ sin(6\alpha)] \tag{8}$$

where n_{nb} is the number of neighbors in contact with the i^{th} particle, $j = \sqrt{-1}$, and α is the angle of the line segment joining the particle and its neighbor's centers, with respect to the X-axis. The overall local order parameter is represented in this work purely as the magnitude of ψ_i. The global order parameter (Ψ) is the average of the local order parameters over all the particles in the domain and is correlated to the dilation boundaries in the domain. Higher values of the global order parameter suggest better packing with respect to the neighboring particles.

3 Results and Discussion

We discuss the results of exercising the model discussed in the previous section hereunder. The results are classified into three parts, (a) Mixing of monodisperse particles, (b) Mixing of bidisperse particles and (c) Mixing of polydisperse particles.

3.1 Flow patterns and mixing process

3.1.1 Mixing of mono disperse particles

The patterns emerging from mixing monodisperse wet particles are shown in Fig. 1 for different time instants. The belt is impulsively started with a velocity of 0.5 after an initial gravitational settling time of $\tau = 12.5$. τ is dimensionless time based on the time scale associated with the belt motion. During this time, the particles settle into a nearly crystalline packing. In order to identify the patterns, we have colored the particles with two different colors (top half of the particles are colored in pink while the bottom half are colored blue). Due to the motion of the belt, the particles near the belt are initiated into motion by the belt. These particles subsequently collide with the particles away from the belt and transfer their momentum. In addition, they collide with the side walls of the enclosure resulting in upward motion before tumbling. These processes can be seen in Fig. 1(b) at $\tau = 62.5$ where the blue particles are surrounded by the pink particles; however, stratification can still be observed. As time progresses, the particles are further mixed, resulting in a nearly well mixed state by the time instant of about $\tau = 500$. The belt-driven enclosure exhibits flow patters reminiscent of the lid-driven cavity. In the current

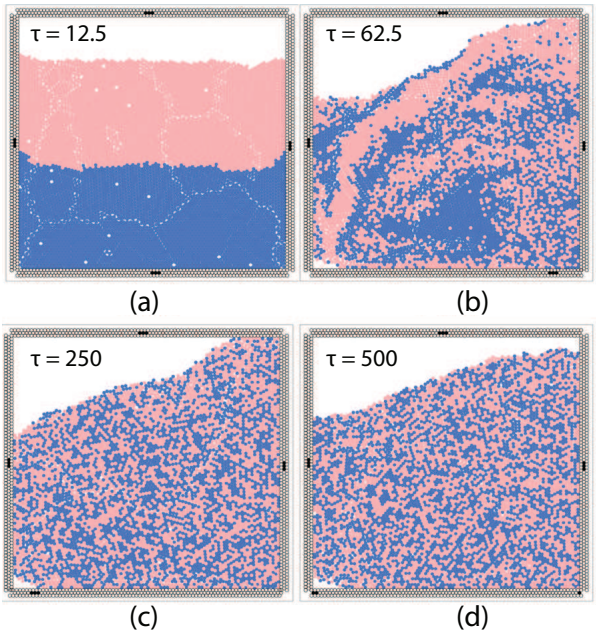

Fig. 1: Mixing of monodisperse particles in the belt-driven enclosure at different time instants. The figure shows that the particles are well-mixed at $\tau = 500$. **Time has been nondimensionalized using a time scale based on cavity dimension and belt speed.**

simulations with purely monodispersed particles, grain-like structures with grain boundaries appear, especially visible at $\tau = 12.5$. These large hexagonally packed regions have been observed to slide against one another. The process of mixing can be found in the supplementary video SM1. As mentioned in the previous section, we define two Mermin order parameters - one in the weak sense and the other in a strong sense to quantify mixing. The local order parameter distribution at a particular time instant signifies the quality of the packing with respect to the neighboring particles. Fig. 2 is a plot of the local order parameter at a time instant of $\tau = 250$ (which is the same instant as in Figure 1 (c)). It should be noted from

this figure that wet granular materials tend to pack into a crystalline arrangement with a few grain boundaries separating large oriented islands. In the present work this kind of situation is observed only for monodispersed particles. The dilation of such islands is one of the major processes through which monodisperse granular material mixes. The energy transfer from the belt to regions in the granular material away from the belt is facilitated by the transfer of force from the belt [35]. This process can be visualized using force lines. Force lines are lines drawn through the centers of the particles which are in direct contact with each other. The length of these lines is an indication of the extent of influence of a given particle. In the case of monodisperse particle systems, these lines appear to extend all the way into the cavity owing to the fact that most of the material is closely packed in an orderly arrangement. Therefore, the motion of the belt is both kinematically and kinetically transferred to the regions away from the belt.

3.1.2 Mixing of bidisperse particles

We now turn our attention to the processes underlying mixing of bidisperse matieral. The mixing of bidisperse particles is shown in Fig. 3 (which is similar to Fig. 1 for the monodisperse case). The overall area fraction of the granular material in the cavity in the bidisperse case is maintained the same as in the previous monodisperse case. The diameter ratio of the smaller particle to the larger particle is 0.5. In addition, the number fraction of the secondary particles (smaller diameter) is 25%. In Fig. 3(b) and (c) the particles are colored by Mermin's local order parameter [34] and by velocity (scaled with belt speed) respectively. The secondary particles of a smaller size are shown as red particles in Fig. 3(a), and as black particles in Fig. 3(b) and (c).

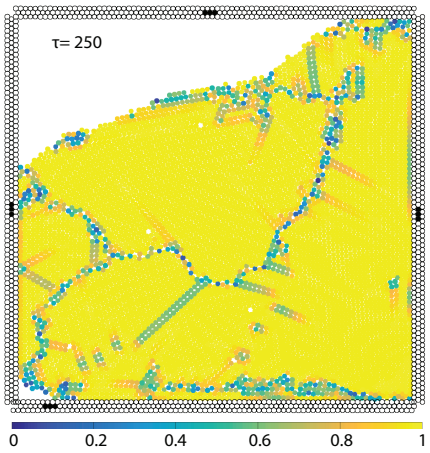

Fig. 2: Mermin's local order parameter [34] variation for monodisperse system. **Particles are coloured by local order parameter [34] (values range from 0 (fluid, loosely packed) to 1 (solid, close packed).** The figure shows the quality of packing with grain boundaries. The white zones shows the voids inside the closely packed particles.

Three observations can be drawn from this figure. Firstly, the mixture composition shown in Fig. 3(a) is significantly better mixed than that shown for monodisperse particles in Fig. 1 at the same time of $\tau = 250$. Secondly, from comparing the Mermin order parameter distribution in Fig. 3(b) to Fig. 2, one can observe that the introduction of the smaller particles appears to break up the long range close-packed structures that were prominent in Fig. 2. The granular matter, under these circumstances, appears to take on a fluidized state which can be seen both in Fig. 3(b) and (c). Fig. 3(c) shows a contour plot of the instantaneous velocity field in the cavity. Lastly, three distinct regions can be observed in Fig. 3(c). A high shear zone can be observed near the belt, a low shear zone (yellow region) can be identified near the right wall of the cavity and a free flowing, cascading layer

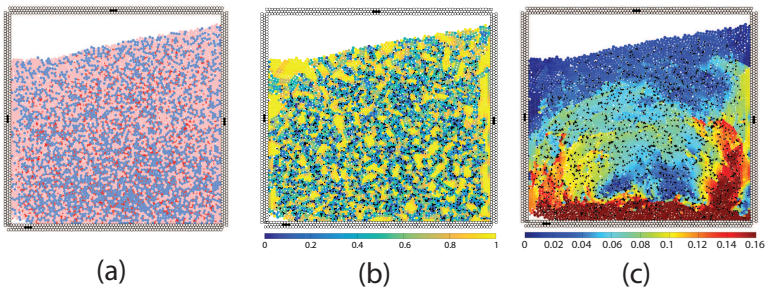

Fig. 3: Particles in the belt-driven enclosure at $\tau = 250$. Bidisperse system, number fraction of secondary particles, $n/N = 0.25$ and $d/D = 0.5$. (a) Vertically stratified layers mixing; (b) Particles coloured by Mermin's local order parameter [34] (values range from 0 (fluid, loosely packed) to 1 (solid, close packed)); (c) Particles coloured by speed contours (scaled with belt speed). The figure shows that after adding the secondary particles the system becomes more fluid-like with less void zones and closely packed structures. Three different fluid zones can be identified from Fig. 3(c): high shear zone near the belt, no flow core zone of the rotating particles and almost stagnant layers of particles above the circulating cell.

of particles can be seen on the free surface. These cascading particles are moving much slower and exhibit much lower shear than the particles near the belt. Owing to these observations, one can conclude that the introduction of a smaller particle tends to promote fluidization in bidisperse granular material. However, an unintended effect of this fluidization is that the force lines in the bidisperse case could be shorter than in the monodisperse case. This results in less effiicient kinematic transfer of wall momentum into the granular material.

3.1.3 Mixing of polydisperse particles

As observed in the previous section, the introduction of an impurity into a monodisperse granular material is beneficial to fluidization; however, momentum transfer becomes less efficient. We now investigate the case where the granular material is polydisperse. The objective is to study the prospect of improving belt momentum transfer while the granular material is in a fluidized state. We have considered three kinds of polydisperse material: (i) uniformly random, (ii) Gaussian random size distribution with the standard deviation being 1% of the mean particle diameter and (iii) Gaussian random size distribution with the standard deviation being 10% of the mean particle diameter. The instantaneous particle configurations of these three cases at a time instant of $\tau = 250$ are shown in Fig. 4(a), (b) and (c), respectively. In all the three cases, the area fraction of the particles in the cavity was maintained the same as in the monodisperse and bidisperse cases. It can be seen from this figure that the mixing of particles is better for lower standard deviation when the particles are in Gaussian distribution. For higher standard deviation smaller size particles tend to segregate mainly due to the percolation. This is further supported by the fact that the void created in the bottom left corner of the cavity for the Gaussian distribution of particles with standard deviation 1% is larger than the other two scenarios shown in Fig. 4.

The free surface of the granular material shows very different pattern for these three different situations in comparison to the other cases discussed previously. The free-surface is highly wavy and shows a higher angle of repose for monodisperse systems. Introducing polydispersity, appears to reduce the angle of repose and produce a free surface largely devoid of cascading waves. This is, again, a

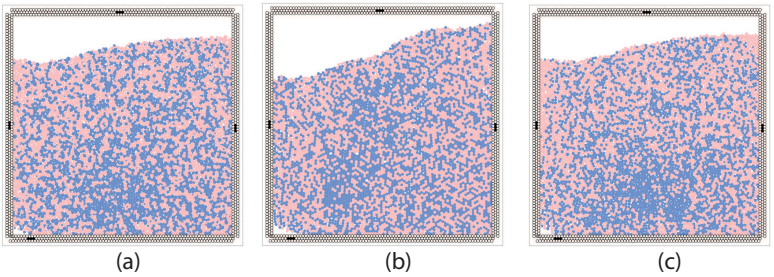

Fig. 4: Polydisperse particles in the belt-driven enclosure at $\tau = 250$. (a) Uniform polydispersed particles with $d_{min} = 2mm$ and $d_{max} = 10mm$; (b) Gaussian distribution of particles with standard deviation 1%; (c) Gaussian distribution of particles with standard deviation 10%. The figure shows that the segregation of particles are different in different conditions whereas, the stable free surface can be observed for uniform polydisperse and Gaussian distribution of particles for standard deviation of 10%.

direct consequence of increased fluidization. Within the three polydisperse cases, the free surface is more unsteady for the 1% standard deviation case shown in Fig. 4(b), since it is the closest to the monodisperse case. The typical mixing of polydisperse particles distributed in the uniformly random fashion can be seen from the supplementary video SM2.

3.2 Quantification of mixedness and crystallinity

We have thus far, presented a qualitative picture of the mixing process. We would like to quantify mixing in order to understand the expense incurred in the mixing process, in terms of time and energy. From the previous discussion, it can be concluded that the overall mixing occurs mainly in three stages, namely, tumbling, inter-penetration and advection. In the tumbling phase, the initially stratified ma-

Table 1: Global order parameter (Ψ) for polydisperse system

	σ/d_m (%)	Ψ
Monodisperse	0	0.9220
Gaussian	1	0.9181
	2.5	0.8946
	5	0.8291
	10	0.6964
Uniform random		0.4429
Bidisperse	Number concentration (n/N in %)	
d/D = 0.3	5	0.8380
	25	0.5900
	50	0.4190
d/D = 0.4	5	0.7990
	25	0.5180
	50	0.4220
d/D = 0.5	5	0.7930
	25	0.5600
	50	0.4550

terial (pink particles at the top, blue particles at the bottom in Fig. 1) becomes more or less vertically stratified. Once the initial top layer (pink particles) reaches the belt, it undergoes horizontal stretching which restores the horizontal distribution around the system's center of mass. The vertical fall does not last long as the pink particles encapsulate the blue particles (Fig. 1) and then the inter-penetration stage commences.

The overall state of packing of the system as well as its mixedness can be identified from the value of the global order parameter of the system. Table 1

presents the average global order parameter for all the situations considered in the present work. It may be recalled that a value of Ψ close to 1 indicates a nearly crystalline (least fluidized) arrangement of the material. As can be noted from the values in Table 1, the system exhibits the highest degree of crystalline packing for the case of a monodisperse particles. Among the bidisperse situations, the global order parameter decreases with an increase in the number concentration (n/N) of the secondary particles. For a constant number concentration, Ψ also appears to decrease with an increase in d/D (except for the very high values of n/N). For the polydisperse situation, the lowest value of Ψ is observed in the uniform polydisperse situation. From these observations, it can be concluded that the presence of secondary particles makes the system less crystalline, resulting in an enhanced fluidization.

The mechanism of enhanced fluidization in the bidisperse and polydisperse cases deserves further discussion. As the bottom belt moves, flow structures similar to separation bubbles in the classical lid-driven cavity become visible in the domain. While this may promise better mixing, segregation effects dominate in these situations. Our results show that while adding secondary particles of a different size aids in the initial stages of mixing by breaking up the crystalline structure. At later times, large segregated zones appear (Fig. 3(b)), which result in an overall poorer state of mixedness. In addition, the mixing which is driven by force line propagation [36, 37] away from the belt become shorter in length. For these two reasons, the initial advantage from enhanced fluidization disappears at later times, especially for high concentrations of the secondary particles.

We now revisit the concept from mixedness by taking both particle size and location into account. For this purpose, the strong mixing parameter is defined

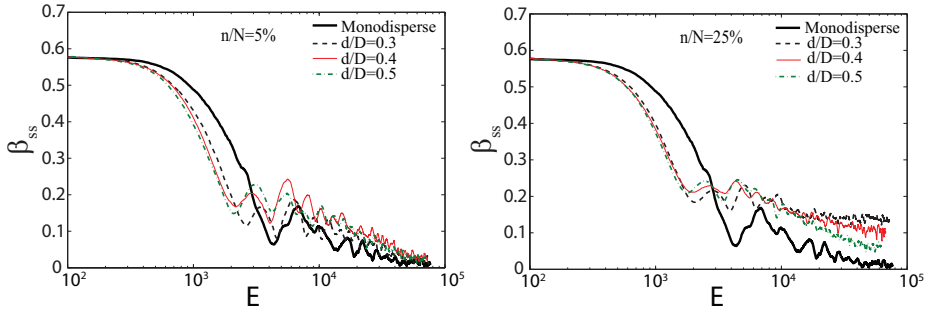

(a)

(b)

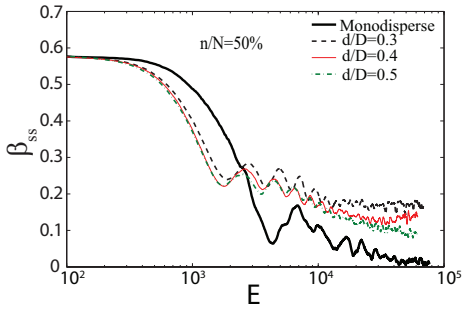

(c)

Fig. 5: Strong sense mixing parameter (β_{ss}) with belt energy input to the system, scaled by belt kinetic energy. Concentration and size effect of secondary particles on mixing; d corresponds to secondary particles' diameter (a) Number concentration = 5%; (b) Number concentration = 25%; (c) Number concentration = 50%. Lower value of strong sense mixing parameter indicates better mixing. It can be seen from the figure that the monodisperse particles are always well mixed.

in Eq. (7). The asymptotic value of the strong mixing parameter is a more clear indicator of the overall mixing in the system. For the purpose of understanding the expense of mixing, we define an energy consumed **up to certain time** in driving the belt as $E = \mathbf{F_D} \cdot \mathbf{v_b}$. Here, $\mathbf{F_D}$ is the total drag force on all the

belt particles and $\mathbf{v_b}$ is the belt velocity. Fig. 5 is a plot of β_{ss} versus the belt energy input (E) for the bidisperse cases. It can be seen from this figure that from an energy perspective, monodisperse systems are more efficient owing to the fact that size segregation is not important. In addition, the kinematic motion of the belt is transferred efficiently to all the granular material. For the other bidisperse systems, the degree of segregation depends on the particle size variability as well as the concentration. A higher concentration of secondary particles causes stronger segregation while a higher diameter ratio of secondary to primary particles favours mixing. Therefore, it appears that a low concentration of secondary particles with their diameter being as close as possible to the mean diameter is favorable. This can be understood more clearly from the strong sense mixing parameter shown in Fig. 6. In Fig. 6 the mixing of bidisperse particles are compared with the monodisperse situation for different concentration of secondary particles at a diameter ratio of 0.5. It can be seen that the strong sense mixing parameter is higher for the more bidisperse case, owing to size segregation.

Figure 7 is a plot of β_{ss} versus belt energy input for the three polydisperse cases. It may be noted that the particle variability is highest for the uniformly random particle size distribution. Consequently, it can be observed from this figure that the uniformly random mixture appears to consume the highest energy to reach the same level of mixedness. In addition, as the standard deviation of the Gaussian distribution increases, the energy require a desired level of mixedness increases. These observations further confirm that mixing is impeded for a broader Gaussian size distributions. This fact is due to the more fluidized state of the material for the high standard deviation Gaussian systems, which is confirmed by the lower global order parameter (See Table 1). The scenario is different though for the case of

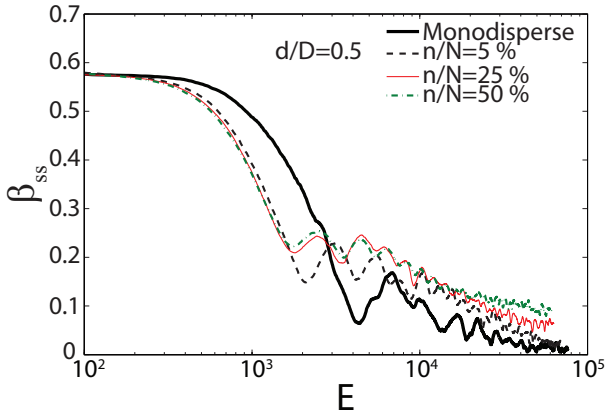

Fig. 6: Strong sense mixing parameter (β_{ss}) with belt energy input to the system, scaled by belt kinetic energy. Different number fraction of secondary particles ($= d/D = 0.5$). The figure depicts that the lower concentration of the secondary particles improves the mixing efficiency of the system.

uniform random distribution of particles. Firstly, the initiation of mixing marked by the system tumbling occurs at a lower energy in these cases. In addition, for the same time period and with the same belt velocity, this granular system consumes lower energy than the Gaussian distribution. Remarkably, it appears to be close to that for a monodisperse system, in spite of the wide distribution of particles. This could be explained by the absence of any window of 'similar' sized particles, unlike the Gaussian or bidisperse system for which such a window clearly exists.

Figure 8 (a) is a plot of the final value of β_{ss} versus the size ratio for bidisperse case. For reference, the monodisperse and uniform polydisperse values are also indicated. From the figure, it can be observed that with an increase of the size ratio for the bi-disperse situations, β_{ss} decreases. For any particular size ratio, β_{ss} increases with an increase of the number

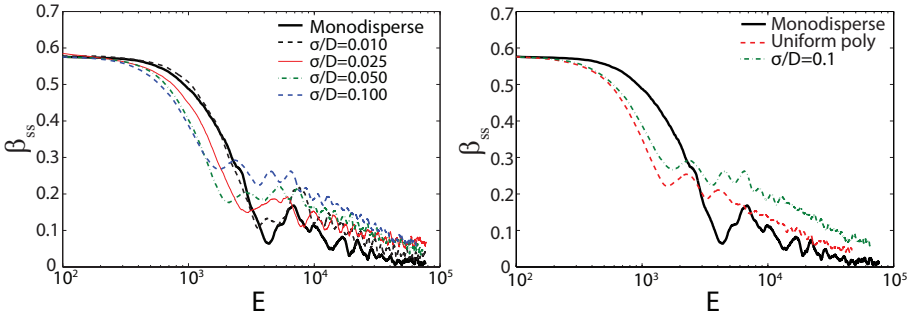

(a) (b)

Fig. 7: Strong sense mixing parameter (β_{ss}) with scaled belt energy. (a) Gaussian distribution: effect of standard deviation (σ/d_m);(b) Size distribution (Gaussian with $\sigma/d_m = 10\%$ and uniform random with $d_{min} = 2mm$ and $d_{max} = 10mm$). The figure shows that the monodisperse system exhibits highest mixing efficiency and for the Gaussian distributed polydispersed system the mixing increases when the standard deviation is lower. The uniformly random polydispersed system tends to reach the monodisperse mixing efficiency.

concentration. As seen in Fig. 8(a), for higher concentration of secondary particles the mixing efficiency decreases (higher value of β_{ss}) below that for uniformly random mixtures. Figure 8 (b) shows the plot of the final value of β_{ss} for Gaussian distributions with different mean particle sizes. It can be noted that the values of β_{ss} in Fig. 8(b) are much lower than those in Fig. 8(a) for bidisperse distributions. Figures 8(c) and (d) show the energy required to obtain the states shown in Fig. 8(a) and (b) for a given composition. The values of the energy for the monodisperse and uniform polydisperse are also shown for reference. For the bidisperse cases, better mixing is obtained at lower energy consumption with increasing size

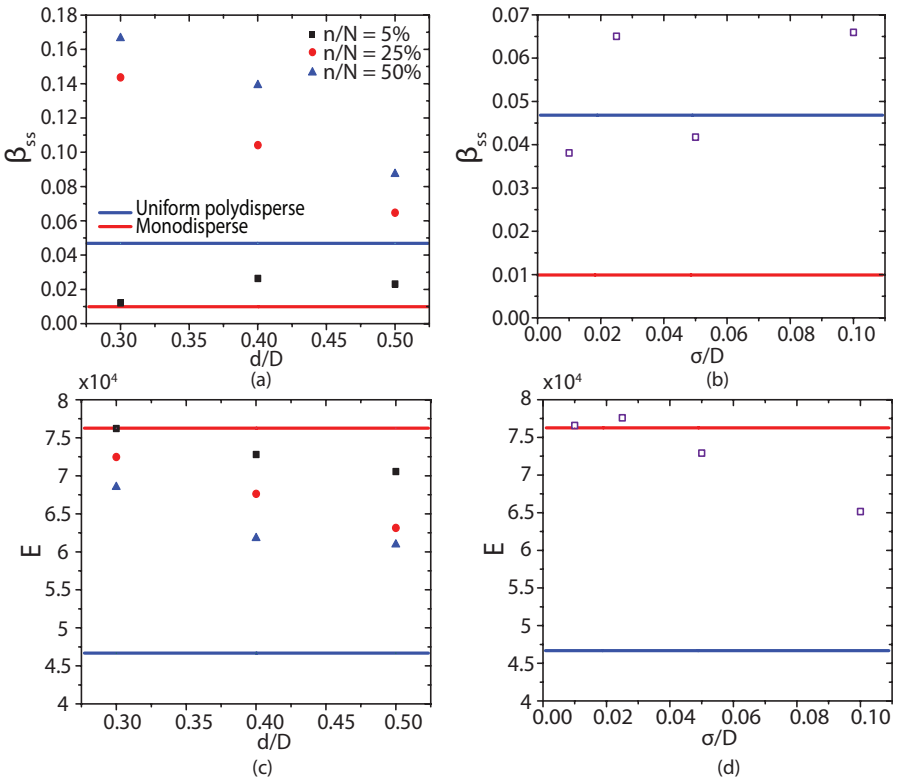

Fig. 8: Final value of the mixing parameter for (a) different size ratios and number concentrations and (b) Gaussian distributions with different standard deviations of the particle sizes. (c) The energy required to obtain the states shown in (a) for different size ratios and (d) the energy required to obtain the state shown in (b) for different Gaussian distribution widths.

ratios. The energy required also decreases with an increase in size ratios and number concentration in the bidisperse case. Figure 8(d) shows the energy required for mixing a granular material with Gaussian distribution of particle sizes as a function of the standard deviation of the particle sizes to achieve the states achieved in Figure 8(b). As can be seen, the energy

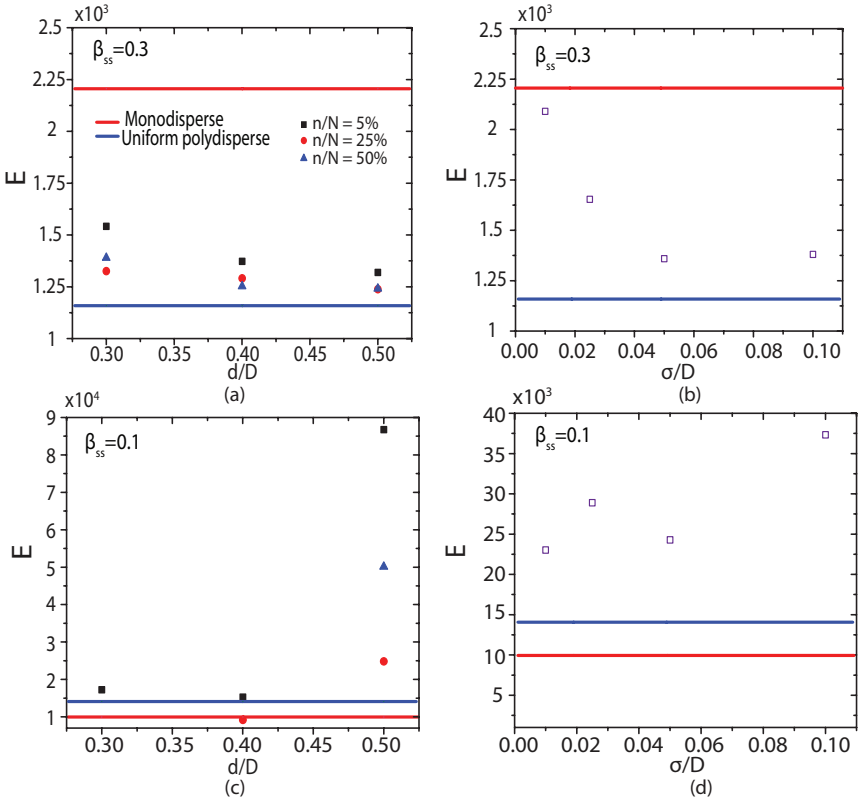

Fig. 9: Energy required for achieving a mixing parameter value of 0.3 for different (a) size ratios and number concentrations and (b) Gaussian distribution widths. Energy required for achieving a mixing parameter value of 0.1 for different (c) size ratios and number concentrations and (d) Gaussian distribution widths.

required decreases with an increasing standard deviation of the particle sizes.

Figure 9 shows the energy required for achieving β_{ss} values of 0.3 and 0.1 for bidisperse and Gaussian distributions of sizes. The energy required to obtain $\beta_{ss} = 0.3$ is lower for increasing size ratios. It is interesting to note that this trend is reversed and greater energy is required to obtain

$\beta_{ss} = 0.1$ as size ratio increases (see Fig. 9(c)). Figure 9(a) also indicates that monodisperse system takes larger energy to achieve $\beta_{ss} = 0.3$ whereas, uniform polydisperse system takes minimum energy. Again, this trend is also reversed in Fig. 9(c). It clearly demonstrates that initial energy requirement to move the monodisperse particles are higher due to the inefficient transfer of kinetic energy to the monodisperse granular system. On the other hand, due to the segregation of particles the energy requirement is less for other parameter conditions. To achieve more efficient mixing ($\beta_{ss} = 0.1$) the final energy requirement for monodisperse system is lowest (as also evident from Figs. 5, 6, 7). It should be noted that the value of $\beta_{ss} = 0.1$ has not been achieved by certain combinations of size concentrations and number ratio (see Fig. 9(c)). Figures 9(b) and (d) are similar to Fig. 9(a) and (c), except that they are obtained with particle sizes following a Gaussian distribution. For all Gaussian distribution cases studied here, the energy required to achieve $\beta_{ss} = 0.1$ is higher than the monodisperse and uniformly random cases. It should be noted that the value of $\beta_{ss} = 0.1$ has not been achieved by certain combinations of size concentrations and number ratio (see Fig. 9(c)).

4 Conclusion

In the present work the mixing of monodisperse and polydisperse wet granular particles are carried out inside a belt driven enclosure. The overall mixing in a belt-driven enclosure seems to be most efficient for a monodisperse system. Introducing secondary particles or size variation may lead to segregation although

it shows promising energy reduction at early stages. The advection stage mixing is observed when segregation occurs wherupon the monodisperse system is more energy efficient than all polydisperse systems. While segregation is prompted by a window of similar sized particles, the study on uniformly white noise random size distribution has revealed close similarity to the monodisperse system for overall mixing at reduced energy costs.

Disclosures

The authors declare that they have no conflicts of interest. The computational resources in the High Performance Cluster was provided by the Indian Institute of Technology Madras. The data in this study was not presented earlier. No human or animal participants have been employed in this study.

References

1. JG Benito and AM Vidales. Novel aspects on the segregation in quasi 2d piles. *Powder Technology*, 234:123–131, 2013.
2. JMNT Gray and C Ancey. Multi-component particle-size segregation in shallow granular avalanches. *Journal of Fluid Mechanics*, 678:535–588, 7 2011.
3. B Remy, J G Khinast, and B J Glasser. Polydisperse granular flows in a bladed mixer: Experiments and simulations of cohesionless spheres. *Chemical Engineering Science*, 66(9):1811–1824, 2011.
4. GR Chandratilleke, AB Yu, and J Bridgwater. A dem study of the mixing of particles induced by a flat blade. *Chemical Engineering Science*, 79:54–74, 2012.

5. O Dube, E Alizadeh, J Chaouki, and F Bertrand. Dynamics of non-spherical particles in a rotating drum. *Chemical Engineering Science*, 101:486–502, 2013.
6. L Devriendt, C Gatumel, and H Berthiaux. Experimental evidence of mixture segregation by particle size distribution. *Particulate Science and Technology*, 31(6):653–657, 2013.
7. D Nguyen, A Rasmuson, I N Björn, and K Thalberg. Cfd simulation of transient particle mixing in a high shear mixer. *Powder Technology*, 258:324–330, 2014.
8. MMHD Arntz, HH Beeftink, WK Otter, WJ Briels, and RM Boom. Segregation of granular particles by mass, radius, and density in a horizontal rotating drum. *AIChE Journal*, 60(1):50–59, 2014.
9. R Collet, D Oulahna, A De Ryck, PH Jezequel, and M Martin. Mixing of a wet granular medium: Influence of the liquid addition method. *Powder Technology*, 208(2):367–371, 2011.
10. A Kudrolli. Granular matter: Sticky sand. *Nature materials*, 7(3):174–175, 2008.
11. SS Hsiau, CC Liao, CH Tai, and CY Wang. The dynamics of wet granular matter under a vertical vibration bed. *Granular Matter*, 15(4):437–446, 2013.
12. K Samiei and B Peters. Experimental and numerical investigation into the residence time distribution of granular particles on forward and reverse acting grates. *Chemical Engineering Science*, 87:234–245, 2013.
13. PY Liu, RY Yang, and AB Yu. Self-diffusion of wet particles in rotating drums. *Physics of Fluids (1994-present)*, 25(6):063301, 2013.
14. GG Pereira and PW Cleary. Radial segregation of multi-component granular media in a rotating tumbler. *Granular Matter*, 15(6):705–724, 2013.

15. A Darelius, J Remmelgas, A Rasmuson, B van Wachem, and IN Bjrn. Fluid dynamics simulation of the high shear mixing process. *Chemical Engineering Journal*, 164(23):418 – 424, 2010. Pharmaceutical Granulation and Processing.
16. PY Liu, RY Yang, and AB Yu. Dynamics of wet particles in rotating drums: Effect of liquid surface tension. *Physics of Fluids*, 23(1):013304, 2011.
17. P Kosinski, A Kosinska, and AC Hoffmann. Simulation of solid particles behaviour in a driven cavity flow. *Powder Technology*, 191(3):327–339, 2009.
18. SJ Tsorng, H Capart, DC Lo, JS Lai, and DL Young. Behaviour of macroscopic rigid spheres in lid-driven cavity flow. *International Journal of Multiphase Flow*, 34(1):76 – 101, 2008.
19. PD Bonkinpillewar, A Kulkarni, MV Panchagnula, and S Vedantam. A novel coupled fluid particle dem for simulating dense granular slurry dynamics. *Granular Matter*, 17(4):511–521, 2015.
20. D Rodrguez, JG Benito, I Ippolito, JP Hulin, AM Vidales, and RO Uac. Dynamical effects in the segregation of granular mixtures in quasi 2d piles. *Powder Technology*, 269:101 – 109, 2015.
21. A Misra and P Poorsolhjouy. Micro-macro scale instability in 2d regular granular assemblies. *Continuum Mechanics and Thermodynamics*, 27(1-2):63–82, 2015.
22. A Leonardi, M Cabrera, FK Wittel, R Kaitna, M Mendoza, W Wu, and HJ Herrmann. Granular-front formation in free-surface flow of concentrated suspensions. *Phys. Rev. E*, 92:052204, Nov 2015.
23. H Yin, M Zhang, and H Liu. Numerical simulation of three-dimensional unsteady granular flows in rotary kiln. *Powder Technology*, 253:138–145, 2014.

24. G Juarez, IC Christov, JM Ottino, and RM Lueptow. Mixing by cutting and shuffling 3d granular flow in spherical tumblers. *Chemical Engineering Science*, 73:195–207, 2012.

25. A Jain, M J Metzger, and B J Glasser. Effect of particle size distribution on segregation in vibrated systems. *Powder Technology*, 237:543–553, 2013.

26. Qingqing Y, Zhiman S, Fei C, and Keizo U. Enhanced mobility of polydisperse granular flows in a small flume. *Geoenvironmental Disasters*, 2(1):1–9, 2015.

27. P Jop. Rheological properties of dense granular flows. *Comptes Rendus Physique*, 16(1):62–72, 2015. Granular physics / Physique des milieux granulaires.

28. M Lätzel, S Luding, and H J Herrmann. Macroscopic material properties from quasi-static, microscopic simulations of a two-dimensional shear-cell. *Granular Matter*, 2(3):123–135, 2000.

29. C Drumm, S Tiwari, J Kuhnert, and H Bart. Finite pointset method for simulation of the liquid–liquid flow field in an extractor. *Computers & Chemical Engineering*, 32(12):2946–2957, 2008.

30. PD Bonkinpillewar, S Vedantam, and MV Panchagnula. Flow of wet granular material in a lid driven cavity. In *Seventh M.I.T. Conference on Computational Fluid and Solid Mechanics*. Massachusetts Institute of Technology, USA, June 2013.

31. WC Swope, HC Andersen, PH Berens, and KR Wilson. A computer simulation method for the calculation of equilibrium constants for the formation of physical clusters of molecules: Application to small water clusters. *The Journal of Chemical Physics*, 76(1):637–649, 1982.

32. S Plimpton. Fast parallel algorithms for short-range molecular dynamics. *Journal of computational physics*, 117(1):1–19, 1995.

33. J Doucet, F Bertrand, and J Chaouki. A measure of mixing from lagrangian tracking and its application to granular and fluid flow systems. *Chemical Engineering Research and Design*, 86(12):1313–1321, 2008.

34. ND Mermin. Crystalline order in two dimensions. *Physical Review*, 176(1):250, 1968.

35. JF Peters, M Muthuswamy, J Wibowo, and A Tordesillas. Characterization of force chains in granular material. *Physical Review E*, 72:041307, 2005.

36. HM Jaeger, SR Nagel, and RP Behringer. Granular solids, liquids, and gases. *Reviews of Modern Physics*, 68:1259–1273, 1996.

37. JM Ottino and DV Khakhar. Mixing and segregation of granular materials. *Annual Review of Fluid Mechanics*, 32:55–91, 2000.